Published in final edited form as:

Nature. 2012 September 13; 489(7415): 313–317. doi:10.1038/nature11316.

HDAC8 mutations in Cornelia de Lange Syndrome affect the cohesin acetylation cycle

Matthew A. Deardorff[1,2,*], **Masashige Bando**[3,*], **Ryuichiro Nakato**[3,*], **Erwan Watrin**[4,*], **Takehiko Itoh**[5], **Masashi Minamino**[3], **Katsuya Saitoh**[3], **Makiko Komata**[3], **Yuki Katou**[3], **Dinah Clark**[1], **Kathryn E. Cole**[6], **Elfride De Baere**[7], **Christophe Decroos**[6], **Nataliya Di Donato**[8], **Sarah Ernst**[1], **Lauren J. Francey**[1], **Yolanda Gyftodimou**[9], **Kyotaro Hirashima**[10], **Melanie Hullings**[1], **Yuuichi Ishikawa**[11], **Christian Jaulin**[4], **Maninder Kaur**[1], **Tohru Kiyono**[12], **Patrick M. Lombardi**[6], **Laura Magnaghi-Jaulin**[4], **Geert R. Mortier**[13], **Naohito Nozaki**[14], **Michael B. Petersen**[9,15], **Hiroyuki Seimiya**[8], **Victoria M. Siu**[16], **Yutaka Suzuki**[17], **Kentaro Takagaki**[18], **Jonathan J. Wilde**[1], **Patrick J. Willems**[19], **Claude Prigent**[4], **Gabriele Gillessen-Kaesbach**[20], **David W. Christianson**[6], **Frank J. Kaiser**[20], **Laird G. Jackson**[1,21], **Toru Hirota**[17], **Ian D. Krantz**[1,2], and **Katsuhiko Shirahige**[3,22]

[1]Division of Human Genetics and Molecular Biology, The Children's Hospital of Philadelphia, USA

[2]The Department of Pediatrics, University of Pennsylvania Perelman School of Medicine, Philadelphia, USA

[3]Research Center for Epigenetic Disease, Institute for Molecular and Cellular Biosciences, The University of Tokyo, Japan

[4]Centre National de la Recherche Scientifique (CNRS), Research Institute of Genetics and Development (IGDR), Faculté de Médecine, Rennes, France

[5]School and Graduate School of Bioscience and Biotechnology, Tokyo Institute of Technology, Yokohama, Japan

[6]Department of Chemistry, University of Pennsylvania, Philadelphia, USA

[7]Center for Medical Genetics, Ghent University Hospital, Ghent, Belgium

[8]Institut für Klinische Genetik, Technische Universität Dresden, Germany

Correspondence and requests for materials should be addressed to I.D.K. (ian2@mail.med.upenn.edu) and K.Sh.(kshirahi@iam.u-tokyo.ac.jp). .

*These authors contributed equally to this work.

Author Contributions M.B. and K.Sh. designed and performed the biochemical analyses; M.B., E.W., C.J., L.M-J and K.Sh performed HDAC screening. K.Sa., E.W. and L.M-J. performed chromatin spreading assays; N.N. monoclonal isolation; R.N., T.I, M.K., Y.K. and K.Sh. the ChIP sequencing and analysis; Y.S. RNA sequencing; M.M., K.T. and T.H. microscopy. M.A.D, G.G.-K., L.G.J, F.J.K and I.D.K. initiated the human studies. M.A.D., D.C., E.D.B., G.R.M., V.M.S., P.W., N.T., Y.G., M.B.P., G.G.-K., and I.D.K. identified and characterized clinical data. M.A.D., M.K., S.E., L.F., M.H. and F.J.K. performed mutation screening, inactivation and lymphoblastoid expression studies. K.H., T.K., H.S. established fibroblast cell lines. M.A.D., J.J.W., K.E.C., P.M.L., C.D. and D.W.C. performed enzymatic and structural analysis. M.A.D., M.B. and K.Sh. drafted the manuscript. All authors analyzed data, discussed the results and commented on the manuscript.

Author Information The authors declare no competing financial interests.

ChIP-Seq and RNA-Seq data from this study is available from the Sequence Read Archive (SRA) database (http://www.ncbi.nlm.nih.gov/sra) under the accession number SRP011927.

[9]Department of Genetics, Institute of Child Health, Athens, Greece

[10]Division of Molecular Biotherapy, Japanese Foundation for Cancer Research, Tokyo, Japan

[11]Department of Pathology, Japanese Foundation for Cancer Research, Tokyo, Japan

[12]Virology Division, National Cancer Center Research Institute, Tokyo, Japan

[13]Department of Medical Genetics, Antwerp University Hospital, Edegem, Belgium

[14]Bio-Frontier Research Center, Tokyo Institute of Technology, Yokohama, Japan

[15]Department of Clinical Genetics, Aalborg Hospital, Aarhus University Hospital, Aalborg, Denmark

[16]Medical Genetics, University of Western Ontario, London, Ontario, Canada

[17]Graduate School of Frontier Sciences, The University of Tokyo, Japan

[18]Experimental Pathology, Japanese Foundation for Cancer Research, Tokyo, Japan

[19]GENDIA, Antwerp, Belgium

[20]Institut für Humangenetik Lübeck, Universität zu Lübeck, Lübeck, Germany

[21]Department of Obstetrics and Gynecology, Drexel University School of Medicine, Philadelphia, PA

[22]CREST, JST, K's Gobancho, 7, Gobancho, Chiyoda-ku, Tokyo, Japan

Abstract

Cornelia de Lange syndrome (CdLS) is a dominantly inherited congenital malformation disorder caused by mutations in the cohesin-loading protein NIPBL[1,2] for nearly 60% of individuals with classical CdLS[3-5] and in the core cohesin components SMC1A (~5%) and SMC3 (<1%) for a smaller fraction of probands[6,7]. In humans, the multi-subunit complex cohesin is comprised of SMC1, SMC3, RAD21 and a STAG protein to form a ring structure proposed to encircle sister chromatids to mediate sister chromatid cohesion (SCC)[8] as well as play key roles in gene regulation[9]. SMC3 is acetylated during S-phase to establish cohesiveness of chromatin-loaded cohesin[10-13] and in yeast, HOS1, a class I histone deacetylase, deacetylates SMC3 during anaphase[14-16]. Here we report the identification of HDAC8 as the vertebrate SMC3 deacetylase as well as loss-of-function *HDAC8* mutations in six CdLS probands. Loss of HDAC8 activity results in increased SMC3 acetylation (SMC3-ac) and inefficient dissolution of the "used" cohesin complex released from chromatin in both prophase and anaphase. While SMC3 with retained acetylation is loaded onto chromatin, ChIP-Seq analysis demonstrates decreased occupancy of cohesin localization sites that results in a consistent pattern of altered transcription seen in CdLS cell lines with either *NIPBL* or *HDAC8* mutations.

Human SMC3 is acetylated by ESCO1 and ESCO2, homologues of yeast ECO1 and has been shown to be important for the establishment of sister chromatid cohesion[10,11,13,17,18]. Using a monoclonal antibody specific for acetylated SMC3 (SMC3-ac)[18], we found that although total SMC3 levels remain stable throughout the cell cycle, SMC3-ac rapidly disappears during mitosis suggesting coordinated deacetylation (Supplementary Fig. 1).

We therefore used RNA interference-based screening of all known human HDACs and Sirtuins to identify HDAC8 as the vertebrate SMC3 deacetylase (Supplementary Fig. 2). Loss of HDAC8 activity using either *HDAC8* RNAi or the HDAC8-specific inhibitor PCI-34051 (PCI; Fig. 1a,b) does not alter cell cycle progression, but clearly increases SMC3-ac in both soluble and chromatin fractions throughout the cell cycle (Fig.1c lanes 4 and 6, Fig. 1e lanes 18-22, 29-33, Supplementary Fig. 3d lanes 22-28 and 36-42). Nearly all of HDAC8 is present in the soluble fraction in both asynchronous and synchronized cultures (Fig. 1c,e). These data indicate that HDAC8 is present and active throughout the cell cycle, and that soluble SMC3-ac is its deacetylation target, similar to Hos1 in yeast[14-16]. Notably, the increase of SMC3-ac in the soluble fraction in the absence of HDAC8 activity implies that SMC3-ac is able to dissociate from chromatin but fails to be deacetylated. In addition, we unexpectedly observed few sister-chromatid cohesion defects with loss of HDAC8 activity alone (Supplementary Fig. 4).

To understand the role of HDAC8 in genome-wide regulation of cohesin dynamics, we performed ChIP-Seq analysis of synchronized HeLa cells transfected with control or *HDAC8* RNAi (Fig. 2) and immunoprecipitated with either an anti-RAD21 antibody to detect total cohesin or with an anti-SMC3-ac antibody. Although total cellular cohesin shows no decrease (Supplementary Fig. 5a,b), and there is a high degree of overlap between SMC3-ac, cohesin and CTCF[19] localization sites in treated and untreated cells, high read numbers and tight correlations between experimental replicates enabled us to identify a 17% loss of total cohesin localization peaks with reduced HDAC8 activity (Fig. 2a-c, Supplementary Fig. 5d-h). Furthermore, despite using conditions that increase total SMC3-ac more than two-fold (Fig. 1e, Supplementary Fig. 3d), we note a 16% loss of SMC3-ac localization sites with HDAC8 reduction (Fig. 2a-d, Supplementary Fig. 5f-g). Finally, we found that in both control and HDAC8-depleted cells, SMC3-ac preferentially localizes to downstream regions of genes relative to the distribution of RAD21 (Fig. 2c,d, and Supplementary Fig. 5f-g). Together, this data demonstrates decreased occupancy of cohesin localization sites with the loss of HDAC8 activity, an observation similarly noted for *NIPBL* haploinsufficient CdLS cells[20].

With the known role of cohesin regulation in CdLS and the observations that reduction of either HDAC8 or NIPBL lead to decreased cohesin occupancy of localization sites, we hypothesized that *HDAC8* mutations may cause CdLS. We screened this X-linked gene in 154 individuals with CdLS negative for mutations in *NIPBL*, *SMC1A* and *SMC3*, as well as *RAD21*, *STAG2*, *ESCO1*, *ESCO2* and *MAU2/SCC4*. We identified four *de novo* missense mutations and one *de novo* nonsense mutation in *HDAC8* (Supplementary Table 1 and Fig. 3a). In addition, one familial mutation (c.1001A>G; p.H334R) was identified in a boy, his mildly affected sister and his unaffected mother, where the mutant allele was inactivated in her blood. This mutation was also one of the *de novo* mutations in an unrelated girl. None of the mutations were seen in 290 ethnically matched control chromosomes or in 629 individuals of the 1000 Genomes Project[21]. Despite the small numbers and the varied clinical features in females due to random X-inactivation, these children demonstrate growth, cognitive and facial features consistent with those caused by mutations in *NIPBL* (“classical” CdLS). Both expression studies (Supplementary Fig. 6a) and X-inactivation

studies (data not shown) demonstrate complete skewing toward the normal allele in the blood of females with *HDAC8* mutations, indicating strong selection against the mutation. This limited the number of cell lines available for subsequent studies. However, immunoblotting demonstrated minimal HDAC8 protein expression in lymphoblastoid cell lines (LCLs) from a hemizygous boy with a p.G320R mutation as well as the skin fibroblasts from a female Lyonized to express a p.H180R mutant allele (Fig. 3b), indicating protein instability in each case. Consistent with this, assessment of SMC3-ac demonstrates increased levels in both the p.G320R LCLs and the p.H180R fibroblasts, while the total amount of SMC3 (Fig. 3b) and cell cycle distribution for the LCLs are unchanged (Supplementary Fig. 6b).

We expressed the HDAC8 missense mutations in *E. coli*, purified and assayed each for deacetylase activity. These data (Fig. 3c) demonstrate that the p.H180R mutation severely abrogates HDAC8 deacetylase activity, and demonstrate significant activity losses for the p.G320R, p.T311M and p.H334R mutations, consistent with high conservation of each residue and position in the structure of HDAC8–substrate complexes [22,23] (Fig. 3d, Supplementary Fig. 6c-e). Finally, purified wild type, but not mutant HDAC8, can rescue the SMC3 overacetylation seen in *HDAC8* mutant LCLs (Supplementary Fig. 6g,h).

We have previously demonstrated that mutations in *NIPBL*, the primary cause of CdLS, result in consistent, reproducible changes of genes expressed from LCLs derived from individuals with CdLS[20]. Using Nanostring multiplex expression analysis to avoid variation introduced by PCR or RNA amplification-based assessments and a previously validated 32-gene CdLS classifier set[20], we compared expression of LCLs from the male with the p.G320R mutation and from two girls (with the p.H180R and p.H334R mutations) who express only the normal allele in these cells, to 10 normal controls and 12 LCLs with loss of function *NIPBL* mutations. In this assay, the aggregate 32-gene LCL expression profile of the single male with an *HDAC8* mutation strongly correlates with that seen of *NIPBL*-mutant cell lines, while the profile for the two female lines, which express the wild type allele, correlates with normal controls (Fig. 3e). These data support the hypothesis that loss of HDAC8 activity results in widespread transcriptional dysregulation as seen in *NIPBL*-mutated CdLS cells. The loss of cohesin binding sites in both *HDAC8* RNAi-depleted HeLa cells and *NIPBL*-mutant LCLs[20] was also noted in the p.G320R HDAC8 mutant LCLs and fibroblasts derived from the girl with the p.H180R mutation, where small but consistent changes in transcriptional dysregulation were also noted (Supplementary Figs 6a,7,8). Together these data suggest that loss of HDAC8 activity leads to a common pathogenic mechanism for “classical” CdLS that converges on the reduction of bound cohesin complexes.

To further understand the endogenous effect of HDAC8 loss on cohesin, we compared each cohesin subunit in chromatin-bound and unbound fractions in the LCLs with a hemizygous p.G320R mutation versus control LCLs and unexpectedly noted accumulation of RAD21 fragments in HDAC8 mutant cells (Supplementary Fig. 9a, lanes 2,4,6). Using a RAD21 N-terminal-specific antibody, we verified accumulation of the RAD21 N-terminal separase cleavage fragment (RAD21-N) in mutant LCLs, HDAC8 RNAi treated HeLa cells and HDAC8-mutated fibroblasts expressing catalytically inactive HDAC8 versus wild type

HDAC8 (Fig. 4, Supplementary Fig. 9). The accumulation of this cleavage fragment in the chromatin-bound fraction of HDAC8-mutant cells suggests that it may remain bound to the cohesin complex, so we assessed whether RAD21-N co-immunoprecipitates with other cohesin subunits. In HDAC8 mutant cells, RAD21-N co-immunoprecipitates with SMC1A, SMC3, STAG1, and STAG2 (Fig. 4b), strongly suggesting that without functional HDAC8, the cleaved N-terminus of RAD21 remains attached to the cohesin complex, presumably via acetylated SMC3[24]. To further confirm that clearance of cleaved RAD21 is dependent on HDAC8, we performed complementary analyses in synchronized HeLa cells with or without the HDAC8 inhibitor PCI (Fig. 4c,d). These data demonstrate the appearance of the N-terminal and C-terminal RAD21 fragments upon entry into mitosis (marked by H3S10-P) and activation of separase (Fig. 4d, lanes 9-12 and 21-24) as well as their persistence in both soluble and chromatin fractions (Fig. 4d lanes 18-20) when most cells are in G1 phase (data not shown). In contrast, in untreated cells, these cleavage products are predominantly detected in the soluble fraction (Fig. 4d lanes 2-4), and largely disappear 3 h post-release.

We also made several observations regarding HDAC8 activity in the prophase removal of cohesin[25,26]. Loss of HDAC8 activity does not disrupt the prophase pathway of cohesin removal from chromatin, as demonstrated by a consistent reduction of chromatin-bound cohesin in the presence of metaphase inhibitors in either control or PCI-treated cells (Fig. 4d, lanes 13 and 17 vs. 21-24). However, HDAC8 activity is necessary following prophase removal since, in metaphase inhibitor-treated cells, soluble SMC3-ac is markedly increased in the presence of PCI (Fig. 4d, lanes 9-12). Finally, with WAPAL depletion, which diminishes prophase removal of cohesin[18,27,28], we noted that SMC3-ac is substantially increased (Supplementary Fig. 9e).

To test whether other cohesion-promoting proteins might remain associated with SMC3-ac in the absence of HDAC8 activity, we analyzed HeLa and patient-derived cells, which also demonstrated increased retention of Sororin[18,29] and RAD21-N, but not WAPAL, on soluble SMC3-ac (Fig. 4e-g, Supplementary Fig. 9d). Taken together, these data strongly suggest that HDAC8 is necessary for deacetylation of SMC3 following its removal from chromatin in both prophase and anaphase pathways to allow proper dissolution of pro-cohesive elements and allow for recycling of “refreshed” cohesin for the following cell cycle (Supplementary Fig. 10).

In summary, this work demonstrates that HDAC8 functions as a vertebrate SMC3 deacetylase to facilitate renewal of cohesin following its removal from chromatin in prophase or anaphase and that loss of HDAC8 activity results in decreased cohesin at localized sites to cause both cellular and clinical features of CdLS.

METHODS

Antibodies and reagents

Primary antibodies used in this study are as previously described for RAD21 (hSCC1)[19], SMC3-ac[18] and RAD21 (Scc1) N terminus[30]. Antibodies used are as follows: SA1, SA2, SMC1A, HDAC6, HDAC10, SIRT4, SIRT5, SIRT7 were from Abcam (Cambridge, MA); α-Tubulin was from Sigma (Tokyo, Japan); Histone H3(S10P), HDAC1, HDAC2, HDAC3,

HDAC4, HDAC5, SIRT1, SIRT3, SIRT6, SIRT7 and MAD2L1 were from Cell Signaling Technology (Danvers, MA); HDAC7, HDAC11 and SIRT2 were from Millipore (Billerica, MA) and SMC3 was from Bethyl Laboratories (Montgomery, TX). HDAC8 antibodies were purchased Santa Cruz Biotechnology (Santa Cruz, CA) or derived as mouse monoclonal HDAC8 antibody raised against peptide CDAYLQHLQKVSQEGDDDHPDS. PCI-34051 was purchased from Sigma Chemical (St. Louis, MO) or synthesized by Synstar Japan Co. TSA, sodium butyrate (SB) and nicotinamide (Nico) were from Wako Chemical (Osaka, Japan). Suberoyl anilide bishydroxamide (SAHA) was from Toronto Research Chemicals (North York, Ontario, Canada). Nocodazole was from Calbiochem (Darmstadt, Germany).

Cell culture and synchronization

HeLa cells were cultured in DMEM (Invitrogen, Camarillo, CA) supplemented with 0.2 mM L-glutamine, 100 units/ml penicillin, 100 μ/ml streptomycin and 10% FCS. LCLs were cultured in RPMI-1640 supplemented with 0.2 mM L-glutamine, 100 units/ml penicillin, 100 μg/ml streptomycin and 20% FCS. Fibroblasts were cultured in DMEM (Invitrogen) supplemented with 0.2 mM l-glutamine, 100 units/ml penicillin, 100 μg/ml streptomycin and 20% FCS. For cell cycle synchronization, HeLa cells were synchronized by double thymidine arrest (DTA; 14–16 h in the presence of 2 mM thymidine, 8 h release, 16 h in the presence of 2 mM thymidine) and harvested 6 h and 13 h after the second release for enrichment in the G2 phase and in the G1 phase, respectively. For enrichment in prometaphase of mitosis, nocodazole (330 nM) was added 8 h after release from the second thymidine block for 1 or 2 h, and cells were harvested by shake off.

Protein extraction and immunoprecipitations

To obtain total cell extracts, cells were lysed with lysis buffer (20mM Tris-HCl pH8.0, 100mM NaCl, 10mM KCl, 5mM MgCl2, 0.2% NP-40, 10% Glycerol, CompleteTM, phosSTOP) and DNA in the chromatin fraction was digested by the treatment of benzonase (Novagen). To obtain soluble cell extracts the cells were lysed with lysis buffer containing 200mM NaCl and centrifugated at 20,000 × g. Immunoprecipitations were performed using ProteinG magnetic beads conjugated with 5μg antibodies and incubated with the cell extracts for 5hr at 4C. After washing with Lysis buffer, the beads were suspended with SDS-PAGE sample buffer.

RNA isolation and RT-PCR

Total RNA was isolated using Trizol (Invitrogen) and Nucleospin RNA II (Macherey-Nagel, Düren, Germany) following the manufacturer's instructions. Synthesis of cDNA was performed using SuperScript III First-Strand Synthesis System (Invitrogen). cDNA was amplified with KAPA SYBR Fast qPCR kit (Kapa Biosystems, Mowbray, South Africa) on an ABI 7500 Real Time PCR system (Applied Biosystems, Carlsbad, CA). Primer sequences were: *HDAC9* Forward-CTTTGTCAGGTTCCTGCTGTTCTC, Reverse-TTCCTGTTTCCACAAGGCATTTC; *ACTB* Forward-TGGCACCCAGCACAATGAA, Reverse-CTAAGTCATAGTCCGCCTAGAAGCA and *GAPDH* Forward-GCACCGTCAAGGCTGAGAAC and Reverse-TGGTGAAGACGCCAGTGGA.

Immunofluorescence microscopy

HeLa cells grown on 18-mm coverslips were fixed with 4% PFA and permeabilized with PBS containing 0.5% Triton X-100 for 10 min. After blocking with goat serum in PBS, cells were incubated with primary antibodies for SMC3 or SMC3-ac. DNA was stained with DAPI.

Chromatin fractionation

Performed as previously described[31].

Chromosome spreads

Cells treated with nocodazole (100 ng/ml) were harvested by mitotic shake off and hypotonically swollen in 40% PBS/ 60% tap water for 5 min at room temperature. Cells were fixed with Carnoy's solution (methanol:acetic acid=3:1), dropped on glass slides and dried. Slides were stained with 5% Giemsa (Merck, Tokyo, Japan), and washed with water, air-dried, mounted with Entellan (Merck, Tokyo, Japan).

Purification of recombinant HDAC8 and SMC3-ac deacetylation assay

Full-length cDNA of HDAC8 and the enzymatically dead HDAC8 mutant (D101A/Y306F)[22] was subcloned into pFASTBacHT (Invitrogen). The Bac-to-Bac baculovirus expression system (Invitrogen) was used to produce recombinant virus according to the manufacturer's protocol. To express recombinant protein, Sf9 cells were infected with each baculovirus and incubated for 60 hours at 27C. Total cell lysates were prepared using Laemmle SDS buffer and boiling for 5 min. For purification of HDAC8 protein, infected cells were lysed with buffer A (20mM Tris-HCl(pH7.5), 300mM NaCl, 0.1% NP-40,10mM 2-ME). After centrifugation at 3000×g the supernatants were incubated with Ni-NTA beads for 2 h at 4C. The beads were washed with buffer A, washed with buffer B [20mM Tris-HCl (pH7.5), 100mM NaCl, 10% Glycerol 0.05% NP-40, 1mM DTT] and eluted with buffer B containing various concentrate of imidazole (50, 100, 200, 350mM). The elution fractions including HDAC8 protein were collected and concentrated using a Centricon concentrator. For detection of SMC3 deacetylation by HDAC8, solubulized total lysates treated with benzonase or SMC1A immunoprecipitants were used as substrates. Substrates were incubated with rHDAC8 or rHDAC8 mutant in reaction buffer [50mM Hepes-KOH(pH7.4), 10% Glycerol, 10mM KCl, 2.5mM MgCl2, 100mM NaCl , 0.1mM PMSF, 50ng/ml BSA, 0.02% NP-40) for 1 hour at 30C and then boiled with SDS sample buffer.

RNA interference

The siRNA oligonucleotides were annealed according to manufacturer's instruction and used at a final concentration of 100–200 nM. The siRNA transfections were performed using oligofectamine (Invitrogen). Oligonucleotides targeting the firefly luciferase GL2 were used as controls. All siRNA sequences are listed in Supplementary Table 2.

Human Subjects

All individuals enrolled in the study were diagnosed by clinical geneticists experienced in the diagnosis of CdLS to have clinical features consistent with a diagnosis of CdLS. All

patients and family members were enrolled in the study under an Institutional Review Board-approved protocol of informed consent at The Children's Hospital of Philadelphia or the Institut für Humangenetik Lübeck.

Mutation Screening

All genes discussed were screened for mutations in the coding exons and intron-exon boundaries using PCR of genomic DNA followed by sequencing. Primers were designed using ExonPrimer [32]. Primer sequences and PCR conditions are available upon request. Sequencing was performed using BigDye Terminator v3.1 cycle sequencing and analyzed on an ABI 3730 (Applied Biosystems, Carlsbad, CA). All probands were pre-screened and were negative for mutations in *NIPBL, SMC1A* and *SMC3.*

Reference sequences and HDAC8 conservation analysis

RefSeq ID numbers for mRNAs and proteins, respectively, referenced in this work include: HDAC8 (NM_018486, NP_060956), *NIPBL* (NM_133433, NP_597677) and *SMC1A* (NM_006306, NP_006297). HDAC8 protein sequences for human (AAF73428), *Bos taurus* (DAA12953), rat (AAI62023), mouse (CAM17598), *Danio rerio* (NP_998596), *Xenopus laevis* (NP_001085711), *Xenopus tropicalis* deduced from mRNA BC161282, *Drosophila melanogaster* (AAC61494) and for *Saccharomyces cerevisiae* HDAC8-like proteins, HOS2 (NP_011321) and RPD3 (AAT92832) were aligned by the ClustalW method[33] using MacVector software (Accelrys Corp, San Diego, CA).

Mapping mutations to the HDAC8 crystal structures

The identified *HDAC8* mutations were mapped onto the crystal structure data of human HDAC8-substrate complex (PDB accession 3F06[23]) to visualize location with respect to active domains of the protein using Cn3D [34], and PyMol [35] software.

Expression analysis of CdLS 32 gene classifier

Lymphocyte culture, and RNA extraction were performed as previously described[20]. Genes and Nanostring[36] (Seattle, WA) probeset sequences are listed in Supplementary Table 3. For each sample 100 ng of RNA was analyzed. Hybridizations were carried out by mixing 5ul of each RNA sample (normalized to 20 ng/ul) with 20 ul of NanoString nCounter Reporter probes and 5 ul of nCounter Capture probes (30 ul total reaction volume) and incubating the hybridizations at 65°C for 18 hours. Post-hybridization purification, NanoString reporter capture, stretching and imaging was performed as described[36]. To account for differences in assay efficiency the data was normalized to the sum of 6 positive internal control RNA spikes that ranged from 0.125-128fM. Internally normalized data was then subsequently normalized to the geometric mean of the *ACTB* and *RPL19* spike-normalized counts. To assess reproducibility, Pearson's r correlation coefficient was calculated for three technical replicates (average r=0.99986) and 11 biological replicates (average r=0.99675). To define a "CdLS" profile, average expression and standard deviations were calculated for 32 genes using RNA from lymphoblastoid cells lines from 10 normal controls and 12 NIPBL truncating or nonsense mutations. For each patient gene expression assay, the number of deviations in expression from normal was determined and divided by the average *NIPBL*

expression standard deviation. These products were then summed for each gene to give a score representing a sum of deviation from normal in a "CdLS" manner for all 32 genes tested for each patient. The data and calculation results for each step are in Supplementary Data File 1.

Recombinant HDAC8 protein expression and purification from *E. coli*

Identified human *HDAC8* mutations were introduced into a previously described HDAC8-6His-pET20b construct[37] using a QuickChange site-directed mutagenesis kit (Agilent Genomics, Santa Clara, CA). Oligonucleotide sequences are available upon request. HDAC8 was recombinantly expressed in BL21(DE3) *E. coli* cells and purified over Talon resin (Clontech, Mountainview, CA) according to published procedures [23], with minor modifications. Briefly, 50 mL cultures (Luria-Bertani media supplemented with ampicillin (50 μg/L)) were grown overnight and used to inoculate 1 L flasks (minimal media supplemented with ampicillin at 50 μg/L). Cells were grown at 37 °C until OD_{600}~0.5, at which point the cells were induced by the addition of isopropyl β-D-thiogalactopyranoside (0.4 mM final concentration) and $ZnCl_2$ (100 μM final concentration), and grown overnight at 18 °C. The cells were pelleted by centrifugation, resuspended in 25 mL of lysis buffer (50 mM Tris (pH 8.0), 500 mM KCl, 5% glycerol, 3 mM β-mercaptoethanol (BME), 115 μM phenylmethanesulfonyl fluoride), and lysed by sonication on ice. Cell debris was pelleted by centrifugation and the cell-free extract was purified by affinity chromatography (Talon resin, Clontech Labs) using a step gradient (Buffer A: 50 mM Tris (pH 8.0), 500 mM KCl, 5% glycerol, 3 mM BME; Buffer B: 50 mM Tris (pH 8.0), 500 mM KCl, 5% glycerol, 3 mM BME, 250 mM imidazole). The final yield was approximately 8.6 mg/L culture for wild-type HDAC8, 6.7 mg/L for G320R HDAC8, 6.1 mg/L for H334R HDAC8, 5.8 mg/L for H180R HDAC8, and 3.9 mg/L for T311M HDAC8; protein concentrations were determined using the colorimetric Bradford assay[38]. The final purity of each protein sample was better than 90% as determined by SDS-PAGE analysis.

HDAC8 activity was measured using the commercially available Fluor-de-Lys HDAC8 deacetylase substrate and Developer II (Enzo Life Sciences, Plymouth Meeting, PA). All assays were run at 25°C and contained 0.5 μM enzyme and 150 μM substrate in assay buffer [25 mM Tris (pH = 8.2), 137 mM NaCl, 2.7 mM KCl, 1 mM $MgCl_2$]. After 30 minutes, the reactions were quenched by addition of the HDAC8 inhibitor M344 (Sigma Aldrich, 100 μM final concentration) and Developer II. Fluorescence was measured using a Fluoroskan II plate reader (excitation = 355 nm, emission = 460 nm). Product concentration was calculated from raw data using standard curves for substrate and product (Aminomethylcoumarin, Enzo Life Sciences), with the total concentration of substrate and product kept at 150 μM (before dilution with the developer solution). All activity assays were performed in triplicate. Enzyme activities are reported as nmol product·μmol $enzyme^{-1}$·min^{-1}.

Assessment of X-inactivation

X chromosome inactivation (XCI) was determined by evaluating the methylation status of the CAG microsatellite locus at the 5′ end of the (AR) androgen-receptor gene as previously described with modifications [39,40]. Briefly, genomic DNA isolated from peripheral blood

and for each patient, two reaction digests were performed. In one reaction, 1 μg of DNA was digested in 25 μl with the methylation-sensitive restriction enzyme *Hpa*II (New England Biolabs), which cuts the active unmethylated allele. In the other reaction, DNA was incubated in enzyme digest buffer without enzyme. After a 16 hour incubation at 37°C, digestion was terminated by incubation at 65°C for 20 minutes. From each reaction, 2 μl was then amplified by PCR with primers flanking the polymorphic androgen receptor CAG repeat as described [39]; forward 5′-CTGTGAAGGTTGCTGTTCCTCAT -3′; reverse 5′-FAM-TCCAGAATCTGTTCCAGAGCGTGC -3′). ABI3730 Genetic Analyzer and GeneMapper V4.0 software (Applied Biosystems) were used for genotyping analysis. Percent X-inactivation was calculated by dividing the ratio of the allele peak volumes in the *HpaII*-treated by the ratio of the allele peak volumes in the untreated sample. We considered alleles separated by more than 2 CAG repeats as informative [41] and used a cutoff of >80:20% for skewed XCI and >95:5% for extremely skewed XCI.

Fibroblast immortalization and lentiviral transduction

CDL016 fibroblasts were immortalized by exogeneous expression of hTERT. HDAC8 and the enzymatically dead HDAC8 mutant (D101A/Y306F)[22] were cloned into pENTR H1 Gateway vector and recombined with lentivirus vector, pCS-RfA-CG, using the LR reaction (Invitrogen). Recombinant lentiviruses were produced from 293FT cells transfected with CS-CMV-HDAC8 or CS-CMV-HDAC8mut and packaging vectors. The fibroblasts were incubated with recombinant lentiviruses in the presence of 8 μg/ml poly-brene and transduction efficiency was measured using GFP expression.

Chromatin immunoprecipitation and qPCR

Cells were crosslinked with 1% formaldehyde for 10 min, quenched with 125□mM glycine, and prepared for ChIP as previously described[19]. ChIP was performed as previously described using RAD21/SCC1, SMC3-ac, and control antibodies[19]. Briefly, crosslinked cell lysates solubulized by sonication were incubated with protein A or protein G Dynabeads (Dynal) crosslinked with the antibodies for 14 h at 4 °C. After this, beads were washed several times and eluted with elution buffer (50 mM Tris, 10 mM EDTA, 1% SDS) for 20 min at 65 °C. The eluates were incubated at 65 °C overnight to reverse crosslinks and then treated with RNaseA and then with proteinase K. The samples were further purified by phenol-chloroform extraction and an additional purification step using a PCR purification kit (Qiagen). Real-time PCR was performed by using KAPA SYBR Fast qPCR kit (Kapa Biosystems) on an ABI 7500 PCR system (Applied Biosystems). The results were presented as a percentage of input chromatin that was precipitated. Primers used in this study were listed in Supplementary Table 4.

ChIP-seq analyses

DNA from whole cell extracts (WCE) and ChIP fractions was further sheared to an average size of approximately150bp by ultrasonication (Covaris, Woburn, Massachusetts), end-repaired, ligated to sequencing adapters and amplified according to manufacturers instructions (Applied Biosystems SOLiD Library Preparation Protocol). Gel-purified amplified DNA between 100 and 150bp was sequenced on the Applied Biosystems SOLiD

platforms (SOLiD 3 and 5500) to generate single-end 50-bp reads. Sequenced reads of both ChIP and WCE were aligned to the human genome (UCSC hg19) using Bowtie[42] allowing 3 mismatches in the first 28 bases per read (−n3 option). All duplicate reads and those without unique alignment were removed from further analysis. Sequencing, read and mapping data are summarized in Supplementary Table 5. We further analyzed only uniquely aligned reads. Each aligned read was extended to a predicted fragment length of 150bp. Reads were summed in 10bp bins along the chromosome for ChIP and WCE, respectively. To facilitate comparison of detected peaks between different ChIP experiments, we normalized the read number of each bin per million uniquely mapped reads for that chromosome for both ChIP and WCE samples (i.e. read number for each bin * 1,000,000 / total number of reads mapped onto reference genomes). This value was further smoothed with a 500bp width (50 bins). Scanning the genome with a 300 bp (30 bin) sliding window, a one-sided Wilcoxon rank-sum test was performed to estimate the enrichment p-value for each window. The fold enrichment (ChIP/WCE) for each window was also calculated. To call peaks, we employed stringent criteria to identify windows which satisfied both fold enrichment > 3.0 and p-value < 1e-4 criteria for candidate binding sites[43]. To further eliminate uncertain sites, we removed the regions with low ChIP reads using the criteria: 1). the average number of ChIP reads in region / the average number of ChIP reads in the genome < 3.0 or 2). the maximum read intensity in ChIP bins was less than 0.2 per million reads mapped. Peak calling summary statistics are summarized in Supplementary Table 6.

RNA-seq analyses

We prepared 2 replicates for each sample for RNA-Sequencing (Solexa HiSeq2000, Illumina, San Diego, CA). Sequenced RNA reads were aligned to RefSeq RNA database (NM* accession numbers only) using Bowtie[42] allowing three mismatches in the first 28 bases per read (−n3 option), and aligned transcript reads were merged for a single gene. To accomodate transcriptional variants, we used both uniquely- and multiply-aligned reads. Multiply aligned reads were divided equally amongst all locations (N-times matched reads were weighted as 1/N reads). Reads that aligned to reference database more than 10 times were discarded. The expression level of each gene was calculated in RPKM (reads per kilobase per million reads)[44] and normalized by TMM (trimmed mean of M values)[45]. RPKM scores of the two replicates were averaged to calculate the enrichment ratio. Using a 2.5 RPKM threshold, we obtained a total of 9,763 expressed genes (Supplementary Table 7).

Data availability

ChIP-Seq and RNA-Seq data from this study is available from the Sequence Read Archive (SRA) database (http://www.ncbi.nlm.nih.gov/sra) under the accession number SRP011927.

Supplementary Material

Refer to Web version on PubMed Central for supplementary material.

Acknowledgements

We are exceptionally grateful to the individuals and families with Cornelia de Lange Syndrome who participated in this study as well as to the referring physicians and colleagues who have contributed samples and clinical

information. We thank Riken Omics Science Center, Keiko Nakagawa, Shoko Watanabe, Melanie Albrecht and Juliane Eckhold for technical support. We thank Dr. Jan-Michael Peters for the Sororin and RAD21 antibodies. We thank Drs. Frederic Beckouët and Kim Nasmyth for sharing unpublished results. We are indebted to the continued support of the USA and International Cornelia de Lange Syndrome Foundations. This work was supported by National Institutes of Health Grants K08HD055488 (NICHD, M.A.D.), GM49758 (D.W.C.), P01 HD052860 (NICHD; I.D.K.), research grants from the USA CdLS Foundation, institutional funds from the Children's Hospital of Philadelphia, Intramural funding from the University of Lübeck (Schwerpunktprogramm, Medizinische Genetik: Von seltenen Varianten zur Krankheitsentstehung; F.J.K., G.G.K.), Research Program of Innovative Cell Biology by Innovative Technology and Grant-in-Aid for Scientific Research (K.Sh.).

REFERENCES

1. Gillespie PJ, Hirano T. Scc2 couples replication licensing to sister chromatid cohesion in Xenopus egg extracts. Curr Biol. 2004; 14:1598–603. [PubMed: 15341749]
2. Takahashi TS, Yiu P, Chou MF, Gygi S, Walter JC. Recruitment of Xenopus Scc2 and cohesin to chromatin requires the pre-replication complex. Nat Cell Biol. 2004; 6:991–6. [PubMed: 15448702]
3. Gillis LA, et al. NIPBL mutational analysis in 120 individuals with Cornelia de Lange syndrome and evaluation of genotype-phenotype correlations. Am J Hum Genet. 2004; 75:610–23. [PubMed: 15318302]
4. Krantz ID, et al. Cornelia de Lange syndrome is caused by mutations in NIPBL, the human homolog of Drosophila melanogaster Nipped-B. Nat Genet. 2004; 36:631–5. [PubMed: 15146186]
5. Tonkin ET, Wang TJ, Lisgo S, Bamshad MJ, Strachan T. NIPBL, encoding a homolog of fungal Scc2-type sister chromatid cohesion proteins and fly Nipped-B, is mutated in Cornelia de Lange syndrome. Nat Genet. 2004; 36:636–41. [PubMed: 15146185]
6. Deardorff MA, et al. Mutations in cohesin complex members SMC3 and SMC1A cause a mild variant of cornelia de Lange syndrome with predominant mental retardation. Am J Hum Genet. 2007; 80:485–94. [PubMed: 17273969]
7. Musio A, et al. X-linked Cornelia de Lange syndrome owing to SMC1L1 mutations. Nat Genet. 2006; 38:528–30. [PubMed: 16604071]
8. Nasmyth K, Haering CH. Cohesin: its roles and mechanisms. Annu Rev Genet. 2009; 43:525–58. [PubMed: 19886810]
9. Dorsett D. Cohesin: genomic insights into controlling gene transcription and development. Curr Opin Genet Dev. 2011
10. Rolef Ben-Shahar T, et al. Eco1-dependent cohesin acetylation during establishment of sister chromatid cohesion. Science. 2008; 321:563–6. [PubMed: 18653893]
11. Unal E, et al. A molecular determinant for the establishment of sister chromatid cohesion. Science. 2008; 321:566–9. [PubMed: 18653894]
12. Zhang B, et al. Dosage effects of cohesin regulatory factor PDS5 on mammalian development: implications for cohesinopathies. PLoS ONE. 2009; 4:e5232. [PubMed: 19412548]
13. Heidinger-Pauli JM, Unal E, Koshland D. Distinct targets of the Eco1 acetyltransferase modulate cohesion in S phase and in response to DNA damage. Mol Cell. 2009; 34:311–21. [PubMed: 19450529]
14. Beckouet F, et al. An Smc3 acetylation cycle is essential for establishment of sister chromatid cohesion. Mol Cell. 2010; 39:689–99. [PubMed: 20832721]
15. Xiong B, Lu S, Gerton JL. Hos1 is a lysine deacetylase for the Smc3 subunit of cohesin. Curr Biol. 2010; 20:1660–5. [PubMed: 20797861]
16. Borges V, et al. Hos1 deacetylates Smc3 to close the cohesin acetylation cycle. Mol Cell. 2010; 39:677–88. [PubMed: 20832720]
17. Zhang J, et al. Acetylation of Smc3 by Eco1 is required for S phase sister chromatid cohesion in both human and yeast. Mol Cell. 2008; 31:143–51. [PubMed: 18614053]
18. Nishiyama T, et al. Sororin mediates sister chromatid cohesion by antagonizing Wapl. Cell. 2010; 143:737–49. [PubMed: 21111234]
19. Wendt KS, et al. Cohesin mediates transcriptional insulation by CCCTC-binding factor. Nature. 2008; 451:796–801. [PubMed: 18235444]

20. Liu J, et al. Transcriptional dysregulation in NIPBL and cohesin mutant human cells. PLoS Biol. 2009; 7:e1000119. [PubMed: 19468298]
21. A map of human genome variation from population-scale sequencing. Nature. 2010; 467:1061–73. [PubMed: 20981092]
22. Vannini A, et al. Substrate binding to histone deacetylases as shown by the crystal structure of the HDAC8-substrate complex. EMBO Rep. 2007; 8:879–84. [PubMed: 17721440]
23. Dowling DP, Gantt SL, Gattis SG, Fierke CA, Christianson DW. Structural studies of human histone deacetylase 8 and its site-specific variants complexed with substrate and inhibitors. Biochemistry. 2008; 47:13554–63. [PubMed: 19053282]
24. Haering CH, Lowe J, Hochwagen A, Nasmyth K. Molecular architecture of SMC proteins and the yeast cohesin complex. Mol Cell. 2002; 9:773–88. [PubMed: 11983169]
25. Waizenegger IC, Hauf S, Meinke A, Peters JM. Two distinct pathways remove mammalian cohesin from chromosome arms in prophase and from centromeres in anaphase. Cell. 2000; 103:399–410. [PubMed: 11081627]
26. Gimenez-Abian JF, et al. Regulation of sister chromatid cohesion between chromosome arms. Curr Biol. 2004; 14:1187–93. [PubMed: 15242616]
27. Gandhi R, Gillespie PJ, Hirano T. Human Wapl is a cohesin-binding protein that promotes sister-chromatid resolution in mitotic prophase. Curr Biol. 2006; 16:2406–17. [PubMed: 17112726]
28. Kueng S, et al. Wapl controls the dynamic association of cohesin with chromatin. Cell. 2006; 127:955–67. [PubMed: 17113138]
29. Schmitz J, Watrin E, Lenart P, Mechtler K, Peters JM. Sororin is required for stable binding of cohesin to chromatin and for sister chromatid cohesion in interphase. Curr Biol. 2007; 17:630–6. [PubMed: 17349791]

Additional Methods References

30. Hauf S, Waizenegger IC, Peters JM. Cohesin cleavage by separase required for anaphase and cytokinesis in human cells. Science. 2001; 293:1320–3. [PubMed: 11509732]
31. Watrin E, et al. Human Scc4 is required for cohesin binding to chromatin, sister-chromatid cohesion, and mitotic progression. Curr Biol. 2006; 16:863–74. [PubMed: 16682347]
32. Strom T. ExonPrimer. 2006
33. Eddy SR. Multiple alignment using hidden Markov models. Proc Int Conf Intell Syst Mol Biol. 1995; 3:114–20. [PubMed: 7584426]
34. Wang Y, Geer LY, Chappey C, Kans JA, Bryant SH. Cn3D: sequence and structure views for Entrez. Trends Biochem Sci. 2000; 25:300–2. [PubMed: 10838572]
35. Schrodinger LLC. The PyMOL Molecular Graphics System (Version 1.3r1). 2010
36. Geiss GK, et al. Direct multiplexed measurement of gene expression with color-coded probe pairs. Nat Biotechnol. 2008; 26:317–25. [PubMed: 18278033]
37. Gantt SL, Gattis SG, Fierke CA. Catalytic activity and inhibition of human histone deacetylase 8 is dependent on the identity of the active site metal ion. Biochemistry. 2006; 45:6170–8. [PubMed: 16681389]
38. Bradford MM. A rapid and sensitive method for the quantitation of microgram quantities of protein utilizing the principle of protein-dye binding. Anal Biochem. 1976; 72:248–54. [PubMed: 942051]
39. Allen RC, Zoghbi HY, Moseley AB, Rosenblatt HM, Belmont JW. Methylation of HpaII and HhaI sites near the polymorphic CAG repeat in the human androgen-receptor gene correlates with X chromosome inactivation. Am J Hum Genet. 1992; 51:1229–39. [PubMed: 1281384]
40. Wang X, et al. Mutations in X-linked PORCN, a putative regulator of Wnt signaling, cause focal dermal hypoplasia. Nat Genet. 2007; 39:836–8. [PubMed: 17546030]
41. Amos-Landgraf JM, et al. X chromosome-inactivation patterns of 1,005 phenotypically unaffected females. Am J Hum Genet. 2006; 79:493–9. [PubMed: 16909387]
42. Langmead B, Trapnell C, Pop M, Salzberg SL. Ultrafast and memory-efficient alignment of short DNA sequences to the human genome. Genome Biol. 2009; 10:R25. [PubMed: 19261174]

43. Katou Y, et al. S-phase checkpoint proteins Tof1 and Mrc1 form a stable replication-pausing complex. Nature. 2003; 424:1078–83. [PubMed: 12944972]

44. Mortazavi A, Williams BA, McCue K, Schaeffer L, Wold B. Mapping and quantifying mammalian transcriptomes by RNA-Seq. Nat Methods. 2008; 5:621–8. [PubMed: 18516045]

45. Robinson MD, Oshlack A. A scaling normalization method for differential expression analysis of RNA-seq data. Genome Biol. 2010; 11:R25. [PubMed: 20196867]

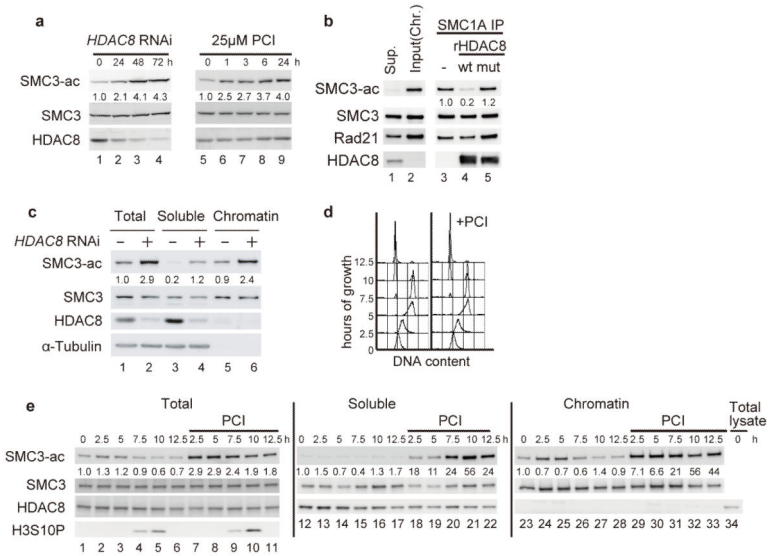

Figure 1. HDAC8 is an SMC3 deacetylase

a, HeLa cells were transfected with *HDAC8* siRNA (Lanes 1-4) or incubated with 25 μM PCI, the HDAC8-specific inhibitor (Lanes 5-9) for the indicated times. Total cell lysates were prepared and analyzed by immunoblotting using anti-SMC3-ac, SMC3 and HDAC8 antibodies. Numbers beneath SMC3-ac bands indicate quantification of SMC3-ac levels normalized to SMC3 levels and the 0 hour time point. **b,** Acetylated SMC3 was prepared by co-immunoprecipitation with SMC1A from HeLa cell chromatin extracts. Immunoprecipitates were incubated with recombinant purified HDAC8 or mutant HDAC8 protein at 30°C for 1 h and analyzed by immunoblotting as in (a). **c,** Unsynchronized HeLa cells transfected with *HDAC8* siRNA for 48 h were fractionated into soluble and chromatin fractions and immunoblotted as in (a). **d,** HeLa cells were synchronized by double thymidine arrest and released into the presence or absence of 25 μM PCI for the indicated time and verified by FACS analysis for cell cycle progression. **e,** Cell extracts of the PCI-treated cells in (d) were fractionated into soluble and chromatin fractions and were analyzed by immunoblotting as in (a). Histone H3 Serine 10 phosphorylation (H3S10P) is a marker of prophase and the onset of mitosis.

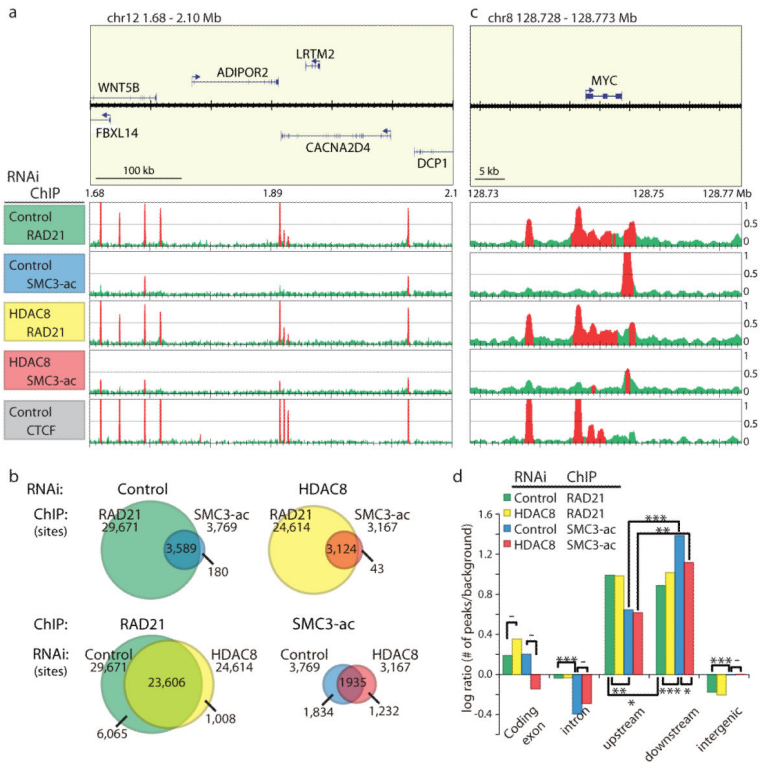

Figure 2. Cohesin and SMC3-ac localization sites in control- and HDAC8 RNAi-treated HeLa cells

a, Example of ChIP-Seq data (Ensemble Gene position 1.68–2.10 Mb of human chromosome 12). ChIP-Seq data are shown in reads per million. Regions in which signals were significantly enriched (see Methods) are in red. Binding profiles for RAD21 and acetylated SMC3 in control and *HDAC8* RNAi-treated HeLa cells are shown. **b,** Venn diagrams showing numbers and overlap of localization sites. **c,** Example of region-specific localization showing RAD21 and SMC3-ac binding sites in the *MYC* gene locus. Ensemble Gene position 128.728-128.773 Mb of human chromosome 8 is shown. **d,** Classification of RAD21 and SMC3-ac localization sites as a log ratio to background reads. Significance was calculated using a 2-sample test for equality of proportions; *, **, *** and -, indicate $p<0.05$, $p<0.001$, $p<0.0001$ and $p>0.05$, respectively. “Upstream” and “downstream” are defined as within 5kb from gene boundaries, respectively. Acetylated SMC3 preferentially localizes to the downstream end of genes.

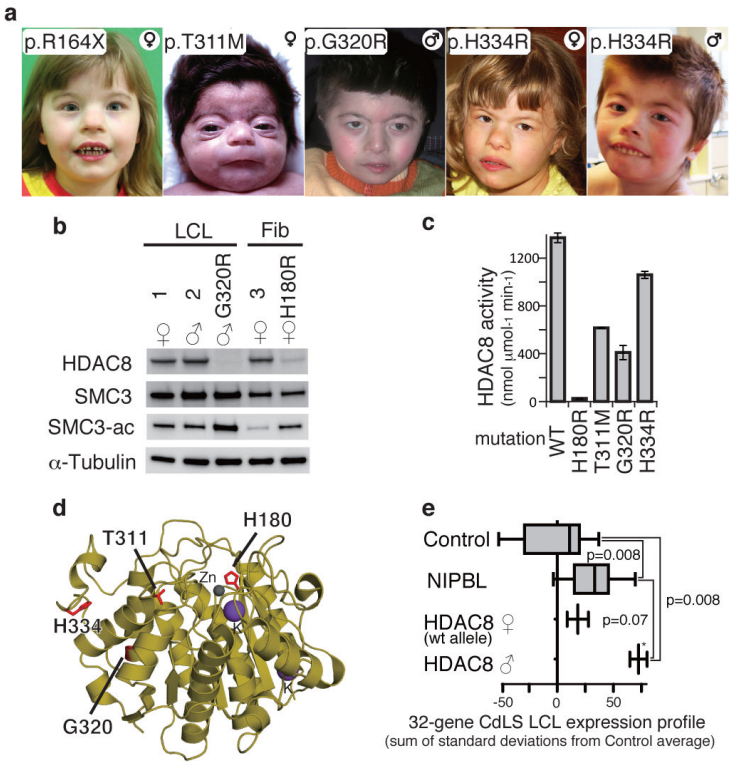

Figure 3. HDAC8 mutations in CdLS

a, Facial features of individuals with *HDAC8* mutations labeled with corresponding mutation and sex; ♂=male, ♀=female**. b,** Western blotting of protein from lymphoblastoid cell lines (LCL) and fibroblasts (Fib). Sex is indicated under Controls (1,2,3) or mutation designation. Primary antibody is indicated at the left. **c,** HDAC8 mutations disrupt deacetylase activity. Bar graphs demonstrate the effect of HDAC8 mutations on deacetylase specific activity (nmol substrate. µmol enzyme^{-1}. min^{-1}). All assays were performed in triplicate. Error bars indicate standard deviation. Enzymatic activity for all mutations is significantly less than wild type ($p<0.05$). **d,** Localization of HDAC8 mutations on the crystal structure (PDB accession code 3F06[23]). Mutated residues are in red. **e,** Expression profile of HDAC8-mutant LCL is consistent with that seen in those with *NIPBL* mutations. The summed standard deviations of gene expression compared to *NIPBL*-mutant from control LCLs for 32 genes was determined for each sample. Box graphs demonstrate 25th, median and 75th percentiles of each group. Whiskers indicate minimum and maximum values. Note that for the HDAC8 male (p.G320R) the values are for biological replicate samples for a single cell line (denoted by *). Unpaired two-tailed t test significances are indicated.

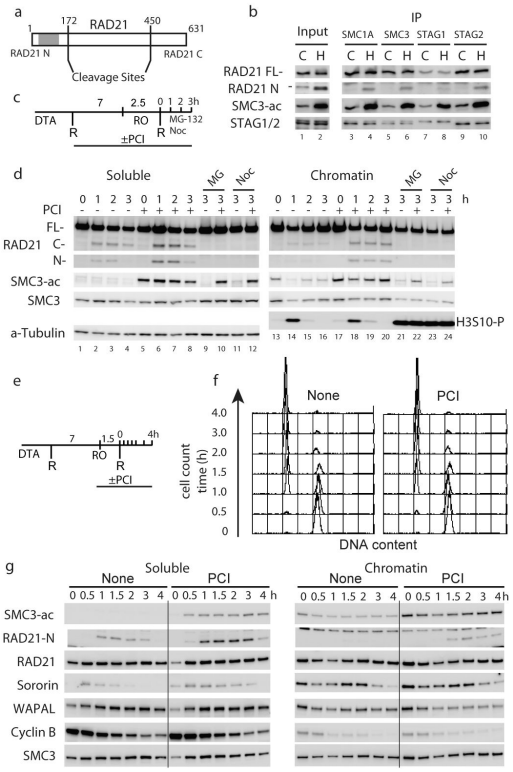

Figure 4. Retention of RAD21-N and Sororin on cohesin in the absence of HDAC8

a, RAD21 separase cleavage sites. Vertical lines indicate cleavage sites. Gray region indicates the RAD21-N antibody epitope. **b,** SMC3, STAG1 and STAG2 were immunoprecipitated from soluble extracts from normal (C) and HDAC8-mutant (H) cell lines. Full-length RAD21 (FL), the cleaved N-terminal fragment of RAD21 (N), acetylated SMC3 (SMC3-ac), and STAG1/2 were analyzed by SDS-PAGE and immunoblotting. **c,** Experimental schema of panel (d). HeLa cells were synchronized by double thymidine arrest (DTA) and released (R) into the presence or absence of PCI. Seven hours after release, cells were treated with RO-3306 (RO) to arrest at the G2/M boundary. After removing RO-3306, cells were cultured in the presence or absence of nocodazole (Noc) or MG-132 (MG) to arrest in metaphase. Cells were harvested at indicated time points after release from RO-3306 arrest. **d,** Cell extracts were fractionated into soluble and chromatin-bound fractions. Full length RAD21 (FL), cleaved C-terminus fragment of RAD21 (C), cleaved N-terminus fragment of RAD21 (N), acetylated SMC3 (SMC3-ac), SMC3, phosphorylated Histone H3 at Serine 10 (H3S10-P), and α-Tubulin were analyzed by SDS-PAGE and immunoblotting. H3S10-P is used as a metaphase marker. **e,** Experimental schema of panel F and G. HeLa cells were synchronized and released and treated with RO-3306 (RO) as in D. After removing RO-3306, cells were cultured in the presence or absence of PCI and harvested at the indicated times. **f,** FACS analysis of HeLa cells in (g). **g,** Cell extracts were fractionated into soluble and chromatin-bound fractions. Levels of SMC3-ac, RAD21-N, full length RAD21 (FL), Sororin, WAPAL, and Cyclin B (a G2 marker) and SMC3 were analyzed by SDS-PAGE and immunoblotting.